

# Degradation-mediated cellular traction directs stem cell fate in covalently crosslinked three-dimensional hydrogels

Sudhir Khetan, Murat Guvendiren, Wesley R. Legant, Daniel M. Cohen, Christopher S. Chen and Jason A. Burdick\*

**Although cell–matrix adhesive interactions are known to regulate stem cell differentiation, the underlying mechanisms, in particular for direct three-dimensional encapsulation within hydrogels, are poorly understood. Here, we demonstrate that in covalently crosslinked hyaluronic acid (HA) hydrogels, the differentiation of human mesenchymal stem cells (hMSCs) is directed by the generation of degradation-mediated cellular traction, independently of cell morphology or matrix mechanics. hMSCs within HA hydrogels of equivalent elastic moduli that permit (restrict) cell-mediated degradation exhibited high (low) degrees of cell spreading and high (low) tractions, and favoured osteogenesis (adipogenesis). Moreover, switching the permissive hydrogel to a restrictive state through delayed secondary crosslinking reduced further hydrogel degradation, suppressed traction, and caused a switch from osteogenesis to adipogenesis in the absence of changes to the extended cellular morphology. Furthermore, inhibiting tension-mediated signalling in the permissive environment mirrored the effects of delayed secondary crosslinking, whereas upregulating tension induced osteogenesis even in the restrictive environment.**

Adhesive interactions with the extracellular matrix direct many aspects of cell behaviour, including viability<sup>1–3</sup>, morphogenesis<sup>4,5</sup> and differentiation<sup>6,7</sup>. As such, it is important to understand interfacial interactions between stem cells and biomaterials towards their utility in therapeutic applications. For cells seeded on hydrogels, the modulus of the substrate can influence stem cell spreading, traction generation and fate<sup>8–10</sup>, also in the absence of soluble differentiation factors<sup>11</sup>. Beyond the modulus, stem cell fate atop two-dimensional (2D) substrates can also be directed by geometric constraints on cell adhesion, which restricts cell spreading and tension generation<sup>12–15</sup>. Despite these advances, the influence of biophysical properties on stem cell fate when presented with a 3D environment is not well understood. It was recently shown<sup>16</sup> that within non-degradable, ionically crosslinked alginate hydrogels, encapsulated MSC differentiation is dictated by matrix stiffness irrespective of cell morphology because MSCs remained rounded independently of stiffness. Specifically, despite the lack of hydrogel degradation, the physically crosslinked alginate was adequately mobile to enable cellular reorganization of bound adhesive ligands, traction generation and differentiation, with magnitudes and fate dependent on hydrogel crosslink density (that is, matrix stiffness). However, many hydrogels behave quite differently from physically crosslinked alginate hydrogels on a molecular level. For example, covalently crosslinked hydrogels exhibit bonds that are stable rather than dynamic. Given the significant amount of work using covalently crosslinked hydrogels for stem cell encapsulation<sup>17–22</sup>, it is important to understand how differences in hydrogel structure and behaviour modulate encapsulated stem cell fate. The work presented here reveals that fate is regulated by cell-generated tension that is enabled through cell-mediated degradation of the covalently crosslinked matrix, and emphasizes that the mechanisms by which stem cells respond to biophysical cues are highly dependent on the type of hydrogel used.

To assess the influence of crosslink density in covalently crosslinked hydrogels on encapsulated hMSC fate (cultured in a bipotential adipogenic/osteogenic media formulation), we replicated the experiment performed in physically crosslinked alginate gels with photopolymerized RGD-modified methacrylated hyaluronic acid (MeHA) hydrogels (Fig. 1a), where hydrogel moduli were tuned by MeHA macromer concentration<sup>23,24</sup>. In contrast to the crosslink-density-dependent response within alginate gels, hMSCs in MeHA gels of all moduli (~4–91 kPa) underwent almost exclusively adipogenesis relative to osteogenesis, as visualized by dual histological staining (Fig. 1b) and quantification (Fig. 1c) for alkaline phosphatase (ALP; osteogenesis) and neutral lipids (adipogenesis). Staining for nuclei confirmed that the lipid droplets corresponded to single cells rather than clusters (Supplementary Fig. S1). When hMSCs were blocked for CD44 interactions with HA through incubation with primary antibodies before encapsulation into MeHA hydrogels, or when untreated hMSCs were encapsulated within methacrylated alginate (MeAlg) or methacrylated dextran (MeDex) hydrogels that lack any HA moieties, the same trend in differentiation was observed across a similar range of mechanics (~4–95 kPa; Supplementary Fig. S2), including at an elastic modulus corresponding to osteogenesis in the physically crosslinked alginate system (~20 kPa; Fig. 1f). These findings suggest that the hydrogel structural cues resulting from covalent crosslinking, rather than direct interactions with the HA chemistry itself, mediate hMSC behaviour and fate.

hMSCs transfected with a green fluorescent protein (GFP)-tagged vinculin reporter and stained for actin showed both limited focal-adhesion formation and diffuse, unpolymerized actin that decreased in expression throughout the 7 d culture (Supplementary Fig. S3). In contrast, hMSCs seeded atop MeHA gels of similar elastic modulus (~25 kPa) and presenting the same RGD concentration exhibited punctate focal adhesion

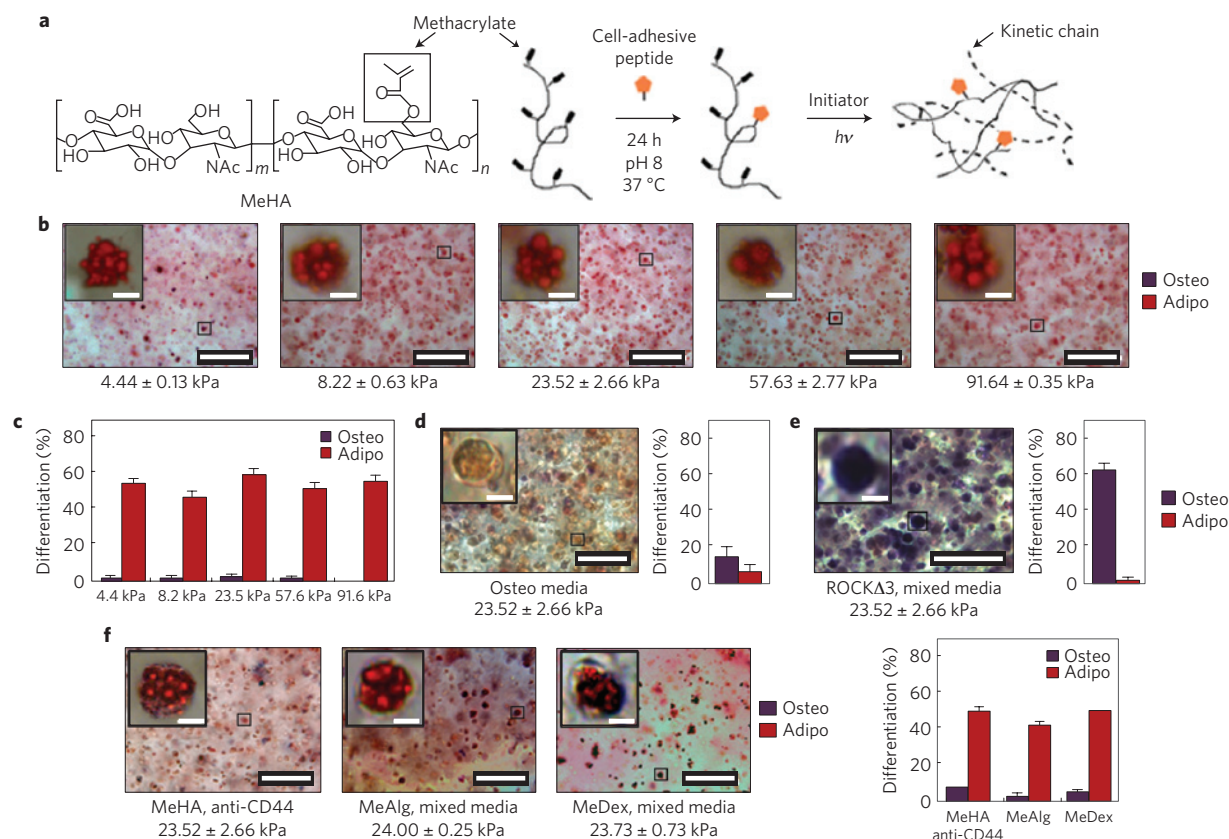


**Figure 1 | hMSC matrix interactions and fate choice within photopolymerized MeHA hydrogels.** **a**, Schematic of RGD conjugation to MeHA and photopolymerization of MeHA. **b, c**, Representative bright-field images (**b**) and percentage differentiation (**c**) of hMSCs within MeHA gels following 7 d mixed osteogenic/adipogenic-media incubation. **d, e**, Representative bright-field images and percentage differentiation of hMSCs within MeHA gels following 7 d osteogenic-media incubation (**d**) or 7 d mixed-media incubation with encapsulated hMSCs transfected with constitutively active ROCK (ROCKΔ3; **e**). **f**, Representative bright-field images and percentage differentiation of hMSCs following 7 d mixed-media incubation within MeHA hydrogels (with hMSCs incubated with primary anti-CD44 antibodies before encapsulation), MeAlg hydrogels or MeDex hydrogels of elastic moduli corresponding to osteogenesis in the physically crosslinked alginate system (~20 kPa). All insets show, in high resolution, a representative single cell from the corresponding lower-magnification bright-field images. For all mixed-media groups, the percentage differentiation was significantly different between osteogenesis and adipogenesis ( $p < 0.001$ ,  $t$ -test). Error bars represent standard error of the mean. Scale bars, 100  $\mu\text{m}$  (**b, d-f**) and 5  $\mu\text{m}$  (insets).

(Supplementary Fig. S4) and underwent primarily osteogenic differentiation<sup>9</sup>. Three-dimensional traction force microscopy<sup>25</sup> (3D TFM) was used to monitor embedded bead displacements and revealed minimal deformation of the surrounding gels by encapsulated hMSCs in all formulations (Supplementary Fig. S5). Cell spreading was quantified as a dimensionless metric termed circularity (ranging from 0 to 1, with values near 0 representing highly spread cells and near 1 representing rounded cells; Supplementary Fig. S6); high hMSC circularity (that is, little spreading) was observed across the range of mechanics (Supplementary Fig. S5). hMSC encapsulation within 23.5 kPa (a modulus that led to osteogenesis in physically crosslinked alginate gels) MeHA gels was then repeated with hMSCs infected with lentivirus containing constitutively active Rho kinase (ROCKΔ3). The ROCKΔ3 hMSCs underwent a fate switch from adipogenesis to osteogenesis (Fig. 1e) despite remaining rounded, suggesting that the formation of load-bearing adhesions toward an osteogenic phenotype can be rescued only by manual activation of tension in a non-degradable, covalently crosslinked hydrogel system. In contrast, when MeHA gels containing non-transfected hMSCs were incubated in osteogenic media alone, little differentiation was observed (Fig. 1d). Taken together, these findings indicate, consistent with previous reports<sup>14,15</sup>, that ROCK-induced cytoskeletal tension is downstream of adhesive and soluble microenvironmental cues and is required for osteogenic versus

adipogenic hMSC differentiation. Further, these results clearly illustrate differences in hMSC adhesion and differentiation based on the type (ionically crosslinked alginate versus covalently crosslinked MeHA) and dimensionality (2D versus 3D) of the hydrogel used.

The above work indicates that crosslink density has little influence on stem cell fate in non-degradable covalently crosslinked systems, even when the network presents adhesive ligands; however, cell-mediated degradation can also be incorporated into these systems through the introduction of proteolytically cleavable crosslinks<sup>26–29</sup>. To accomplish this, HA was functionalized with both methacrylate and maleimide groups (MeMaHA; Fig. 2a; 14% and 10.5% modification, respectively) and subjected to a multi-step crosslinking protocol for cellular encapsulation (Fig. 2b). In the primary crosslinking step, a –UV hydrogel was formed using Michael-type reactions between MeMaHA maleimides and thiols on monofunctional cell-adhesive oligopeptides and bifunctional matrix metalloproteinase (MMP)-degradable peptides (100% theoretical maleimide consumption). In a secondary step, –UV hydrogels were incubated with I2959 photoinitiator and exposed to light to initiate free-radical photopolymerization of methacrylates (D0 UV), introducing kinetic chains that impede proteolytic degradation. <sup>1</sup>H NMR analysis of –UV and D0 UV hydrogels (solubilized by incubation with hyaluronidases) demonstrated that primary and secondary crosslinking consumed all maleimides and methacrylates, respectively (Fig. 2c). When

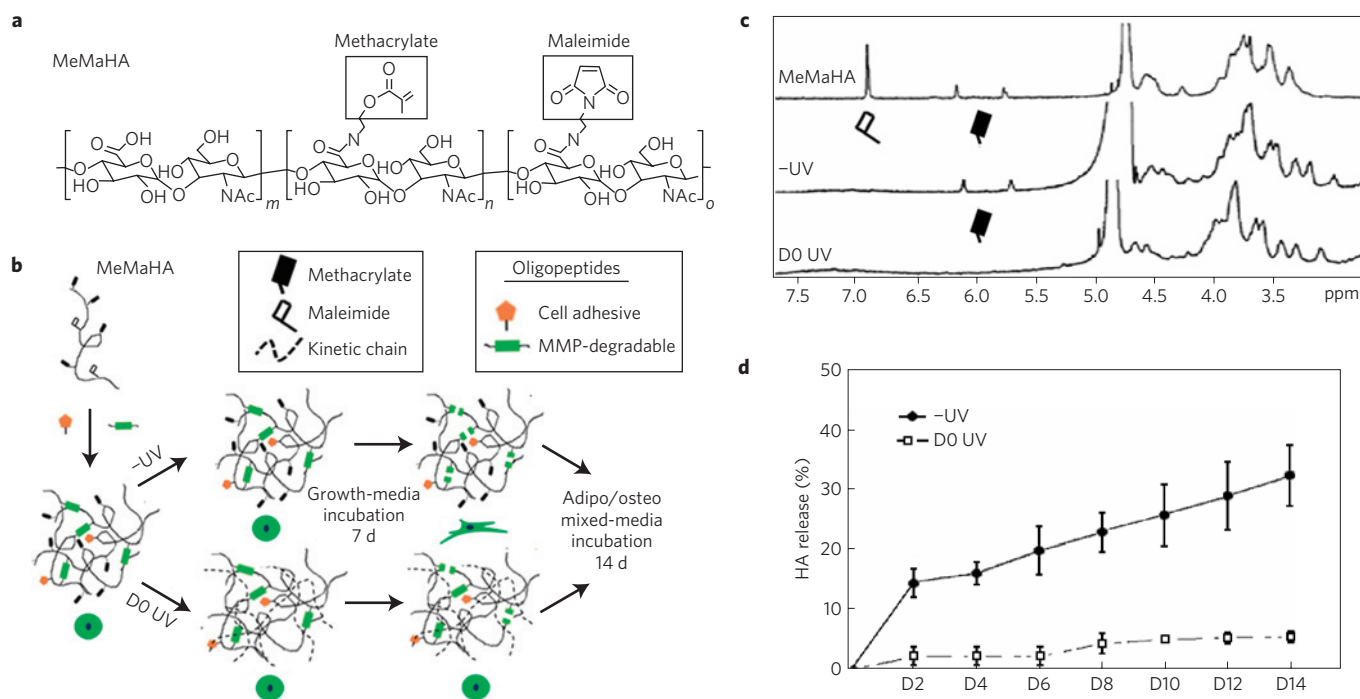


**Figure 2 | Sequential crosslinking characterization and proteolytic degradation kinetics of MeMaHA hydrogels.** **a**, MeMaHA chemical structure ( $m = 0.755$ ,  $n = 0.14$ ,  $o = 0.105$ ). **b**, Schematic of sequential crosslinking of MeMaHA using a primary addition and (nominally) secondary radical polymerization to create -UV and D0 UV hydrogels, respectively. **c**,  $^1\text{H}$  NMR spectra ( $\text{D}_2\text{O}$ ) showing uncrosslinked MeMaHA polymer, -UV and D0 UV hydrogels, respectively. **d**, Degradation kinetics of -UV and D0 UV hydrogels in the presence of 20 nM MMP-2. For all time points, the percentage of HA release was greater from -UV relative to D0 UV gels ( $p < 0.01$ ,  $t$ -test). Error bars represent standard error of the mean.

incubated with 20 nM exogenous MMP-2 for 14 d (Fig. 2d), -UV hydrogels exhibited rapid HA release consistent with proteolytic degradation, whereas D0 UV gels exhibited little HA release. The same trends were observed on incubation of -UV and D0 UV gels with 10 nM membrane type-1 MMP (pro and catalytic form; Supplementary Fig. S7), illustrating that the oligopeptide sequence used in this study is susceptible to degradation by multiple proteases, and that secondary polymerization universally restricts proteolytic degradation. To investigate the influence of cell-mediated degradation on hMSC behaviour, the MeMaHA macromer concentrations used were tuned to provide similar initial elastic moduli for formulations either permissive (-UV) or inhibitory (D0 UV) to cell-mediated degradation (2.5 wt% MeMaHa for -UV hydrogels:  $E = 4.30 \pm 0.11$  kPa; 1.5 wt% MeMaHA for D0 UV hydrogels:  $E = 4.49 \pm 0.18$  kPa).

To assess the importance of local degradability on cell behaviour, hMSCs were uniformly encapsulated by resuspension in the polymer solution immediately before the addition of the crosslinker peptide (Supplementary Fig. S8). At day 7 of growth-media incubation, hMSCs spread within -UV hydrogels and deformed the surrounding matrix to a greater extent than rounded hMSCs within D0 UV gels (Fig. 3a). Bead displacements ( $\sim 7$ -fold greater in -UV versus D0 UV) and cellular circularity ( $\sim 3.5$ -fold greater in D0 UV versus -UV) were found to be significantly different between the gels (Fig. 3b,c). Rheological testing confirmed that bead encapsulation did not alter MeMaHA gelation or the final elastic modulus (Supplementary Fig. S9). Staining for actin demonstrated a robust network of stress fibres within cells in -UV gels, with vinculin concentrated at the tips of extended processes (Fig. 3d). In contrast, only diffuse, depolymerized actin and no organized vinculin were observed within cells in D0 UV gels (Fig. 3e), suggesting that secondary crosslinking restricted hMSC matrix adhesion and cytoskeletal organization as observed in MeMaHA gels. To confirm that this switch was mediated by a change in

degradation cues and was not an adverse effect of light exposure on the hMSCs, cell viability and total DNA content were evaluated in the -UV and D0 UV conditions, as well as in gels exposed to light in the absence of photoinitiator (UV+light) after 7 d growth-media incubation (Supplementary Fig. S10). Similarly high viability was observed in all conditions; furthermore, total DNA content, as well as hMSC circularity, was similar between the -UV and -UV+light groups, indicating that light exposure did not adversely affect the encapsulated hMSCs. Matrix-assisted laser desorption/ionization analysis confirmed that light exposure did not damage the RGD-containing cell-adhesive oligopeptide (Supplementary Fig. S11). Further, the concentration of RGD peptide was quantitatively determined to be equivalent between -UV and D0 UV gels (Supplementary Fig. S12). Encapsulation of hMSCs into MeMaHA gels without RGD peptide resulted in rounded cells exhibiting lower viability and minimal tractions (Supplementary Fig. S13), indicating that the hMSC spreading and traction responses were mediated through integrin-RGD binding. Although this specific ligand may not be necessary for the observed results, adhesion seems to be needed for hydrogel degradation and traction generation. Finally, gene expression and biochemical staining for ALP and lipids indicated that encapsulated hMSCs remained undifferentiated after the growth-media incubation period (Supplementary Fig. S14).

On switching the media to a bipotential adipo/osteo media for 14 days following the 7 d growth-media incubation (that is, for day 7–21 of culture), the same population trends in cell spreading and traction generation were observed (Fig. 3f–h). With respect to differentiation, hMSCs within -UV and D0 UV gels underwent primarily osteogenesis and adipogenesis, respectively, on the basis of dual staining for ALP and lipids (Fig. 3i(ii),j(ii)). Lineage commitment was quantified by counting cells stained for each marker and dividing by total nuclei; osteogenesis was significantly greater in -UV ( $72.4\% \pm 10.0\%$ ) versus D0 UV ( $14.9\% \pm 8.1\%$ ) gels, whereas adipogenesis was significantly greater

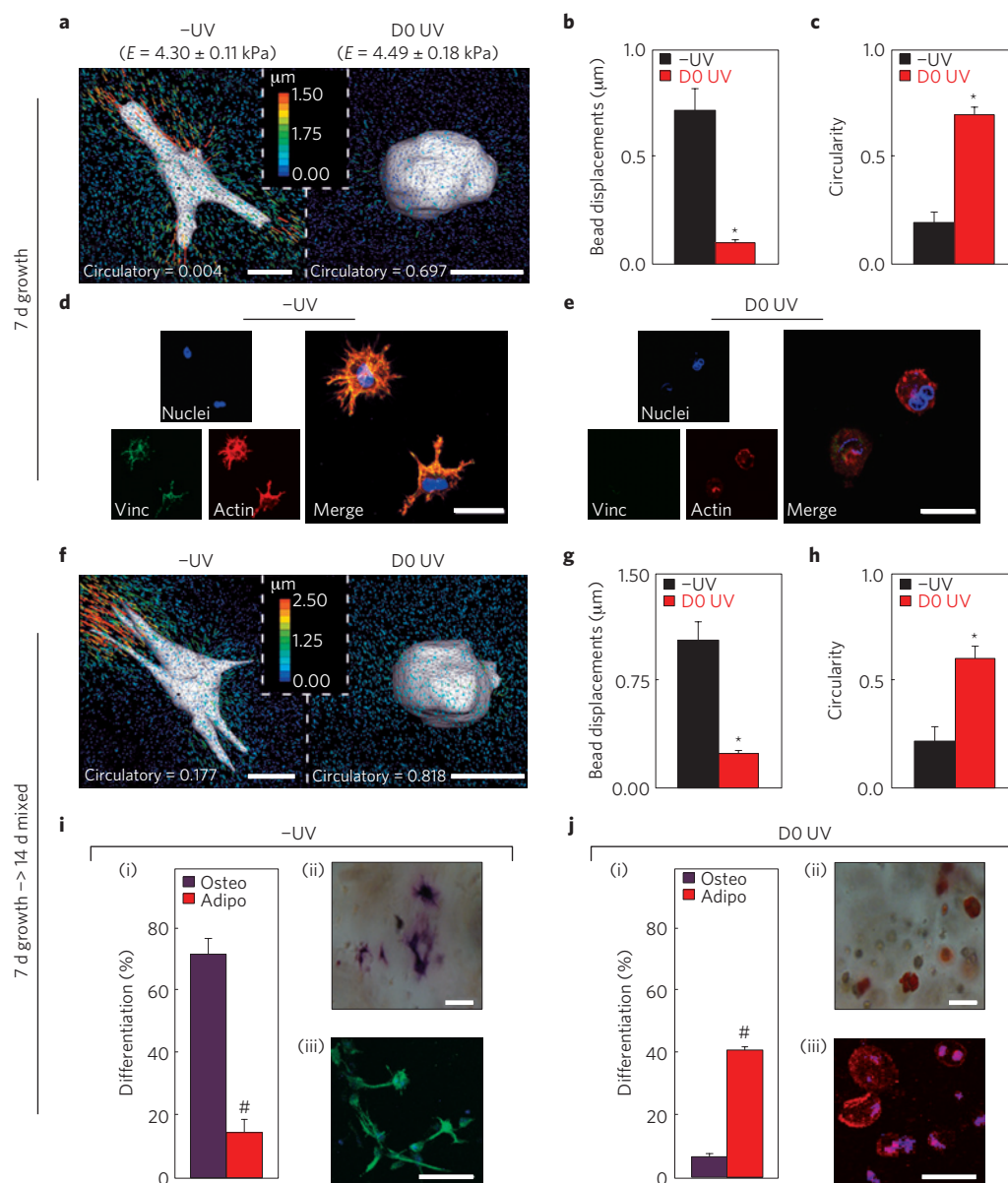


**Figure 3 | MeMaHA hydrogel structure-dependent hMSC matrix interactions and fate choice.** **a–c**, Representative 3D TFM images (**a**), average drift-corrected bead displacements within 15  $\mu\text{m}$  of the cell surface ( $*p < 0.001$ , *t*-test; **b**), and average circularity ( $*p < 0.001$ , *t*-test; **c**) of hMSCs following 7 d growth-media incubation. **d,e**, Representative staining for hMSC vinculin (green), actin (red) and nuclei (blue) in –UV (**d**) and DO UV (**e**) gels. **f–h**, Representative 3D TFM images (**f**), average drift-corrected bead displacements within 15  $\mu\text{m}$  of the cell surface ( $*p < 0.001$ , *t*-test; **g**), and average circularity ( $*p < 0.001$ , *t*-test; **h**) of hMSCs following an additional 14 d mixed-media incubation. **i,j**, hMSC differentiation following an additional 14 d mixed-media incubation. Percentage differentiation of hMSCs towards osteogenic or adipogenic lineages in –UV (**i(i)**) or DO UV (**j(i)**) gels ( $\#p < 0.005$ , *t*-test). Representative bright-field images of hMSC staining for ALP (osteogenesis) and lipid droplets (adipogenesis) in –UV (**i(ii)**) or DO UV (**j(ii)**) gels. Representative immunocytochemistry for osteocalcin (OC, osteogenesis) and fatty acid binding protein (FABP, adipogenesis) of hMSCs in –UV (**i(iii)**) or DO UV (**j(iii)**) gels. Error bars represent standard error of the mean. Scale bars, 10  $\mu\text{m}$  (**a,f**), 15  $\mu\text{m}$  (**d,e**), 25  $\mu\text{m}$  (**i(ii),j(ii)**) and 20  $\mu\text{m}$  (**i(iii),j(iii)**).

in DO UV ( $41.1\% \pm 1.5\%$ ) versus –UV ( $5.5\% \pm 0.3\%$ ) gels. The population differentiation trends were confirmed at day 21 using gene expression (Supplementary Fig. S14) and immunocytochemistry for osteocalcin (OC, osteogenesis) and fatty-acid-binding protein (FABP, adipogenesis; Fig. 3i(iii),j(iii)). Note that there is upregulation for both adipogenic and osteogenic genes in all systems after culture in bipotential media; yet, this translates only to protein staining with the appropriate environmental signals. These same differentiation trends were observed when hMSCs were encapsulated at the seeding density corresponding to 3D TFM studies ( $60,000 \text{ cells ml}^{-1}$ ; Supplementary Fig. S15), confirming that cellular traction generation through matrix adhesion, rather

than cell density and associated cell–cell interactions, directed cell fate. Furthermore, the images acquired for TFM showed uniform embedded bead distributions immediately surrounding the cells; this suggests that hMSC-mediated degradation in this system was localized to the site of initial encapsulation, and that cell motility and migration was not a significant factor. Thus, within hydrogels of the same initial modulus, osteogenesis was favoured in systems where cells were able to spread and pull on the surrounding matrix, and adipogenesis was favoured in systems where cells remained rounded and were unable to displace the surrounding matrix. It is also interesting to note that these moduli are much lower than those that supported hMSC spreading and osteogenesis in 2D (refs 8,9,

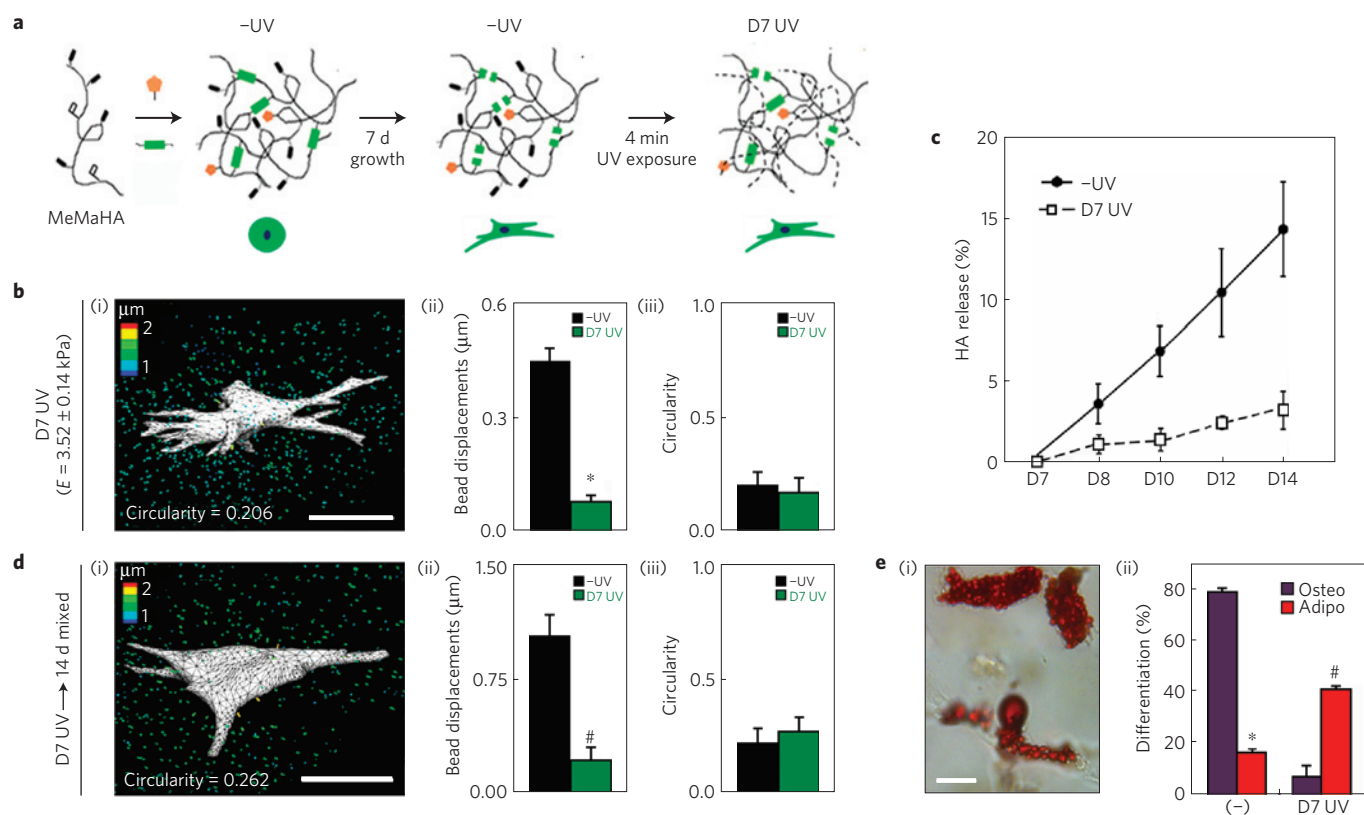


**Figure 4 | Delayed secondary crosslinking redirects hMSC matrix interactions and fate choice without altering cell shape.** **a**, Schematic of delayed UV exposure following 7 d growth-media incubation. **b**, Representative TFM image of a single hMSC (i), hydrogel deformations ( $*p < 0.001$ ,  $t$ -test; (ii)) and circularity (iii) of hMSCs within MeMaHA hydrogels following D7 UV exposure. **c**, HA release from D7 UV versus  $-UV$  hydrogels (normalized to total HA content) in the presence of 20 nM MMP-2. **d**, Representative TFM image of a single hMSC (i), hydrogel deformations ( $\#p < 0.005$ ,  $t$ -test; (ii)) and circularity (iii) of hMSCs within MeMaHA hydrogels following D7 UV exposure and an additional 14 d mixed-media incubation. **e**, Representative bright-field image of a D7 UV hydrogel with encapsulated hMSCs stained for ALP (osteogenesis) and lipid droplets (adipogenesis; (i)), and percentage differentiation within D7 UV hydrogels following 14 d mixed-media incubation ( $*p < 0.001$ ,  $\#p < 0.005$ ,  $t$ -test; (ii)). Error bars represent standard errors of the mean. Scale bars, 25  $\mu\text{m}$  (**b,d**) and 10  $\mu\text{m}$  (**e**).

30,31), again highlighting dimensionality as a biophysical cue that impacts stem cell behaviour.

To decouple the influence of spreading and hydrogel degradation, the MeMaHA system was again used, but the secondary crosslinking was applied at day 7 (D7 UV), after the hMSCs were allowed to spread (Fig. 4a). This delayed crosslinking resulted in a significant increase in the elastic modulus and a significant decrease in bead displacements compared with the same hydrogel formulation without UV exposure (Supplementary Fig. S16). Delayed crosslinking also altered proteolytic degradation of the network; specifically, acellular D7 UV hydrogels exhibited minimal degradation when incubated with 20 nM MMP-2 compared with  $-UV$  gels (Fig. 4c), indicating that delayed crosslinking impedes further proteolytic degradation in a manner similar to D0 UV exposure. Three-dimensional TFM analysis revealed significantly reduced deformations within D7 UV gels 24 h after exposure relative to control gels of the same hydrogel formulation without UV exposure at the same time; however, these gels have different moduli (Supplementary Fig. S16). Bead displacements were also reduced when compared with  $-UV$  gels (Fig. 4b(i,ii)) with similar moduli (2.5 wt% MeMaHA for  $-UV$  hydrogels:  $E = 4.30 \pm 0.11$  kPa; 1.5 wt% MeMaHA for D7 UV hydrogels:  $E = 3.52 \pm 0.14$  kPa following crosslinking) and no differences in cell morphology (Fig. 4b(iii)). Thus, the introduction of non-degradable crosslinks after cell spreading prevented further deformation of the matrix. It was also confirmed that the exposure of hMSCs to UV light itself (that is, in the absence of photoinitiator)

did not affect cellular tractions (Supplementary Fig. S17). Following incubation of the  $-UV$  and D7 UV groups with similar moduli in mixed inductive media for a further 14 days, there was no change in cell traction or morphology (Fig. 4d(i-iii)); however, adipogenesis was significantly increased relative to osteogenesis in the D7 UV hydrogels, resulting in morphologically spread cells with extensive lipid droplet formation (Fig. 4e). Furthermore, hMSCs within the D7 UV gels exhibited minimal cytoskeletal organization, in contrast to robust cytoskeletal organization within  $-UV$  gels (Supplementary Fig. S18). Thus, these findings indicate that the ability of a cell to degrade and interact with the hydrogel during the differentiation stage dictates cellular interactions with the gel and fate decisions, regardless of whether the hMSC is spread.

To further understand the mechanism by which delayed secondary crosslinking abrogates hMSC tractions and redirects fate,  $-UV$  gels were treated with Y-27632, an inhibitor of ROCK, the RhoA effector that induces non-muscle myosin-mediated contractility. Y-27632 (10  $\mu\text{M}$ ) was administered daily during either the 7 day growth-media (day 0–7) or 14 day mixed-media incubation (day 7–21) periods to prevent the assembly of a robust actin cytoskeleton (Fig. 5). When treated with 10  $\mu\text{M}$  Y-27632 daily during the 7 day growth-media incubation, hMSCs deformed the matrix to a much lesser extent (Fig. 5a,c–e), yet exhibited similar spreading (Fig. 5b) to hMSCs without the pharmacological inhibitor treatment. When hMSCs in  $-UV$  gels were treated with Y-27632 only during the differentiation phase (day 7–21), a decrease in gel deformation (Fig. 5f) and no change in cell

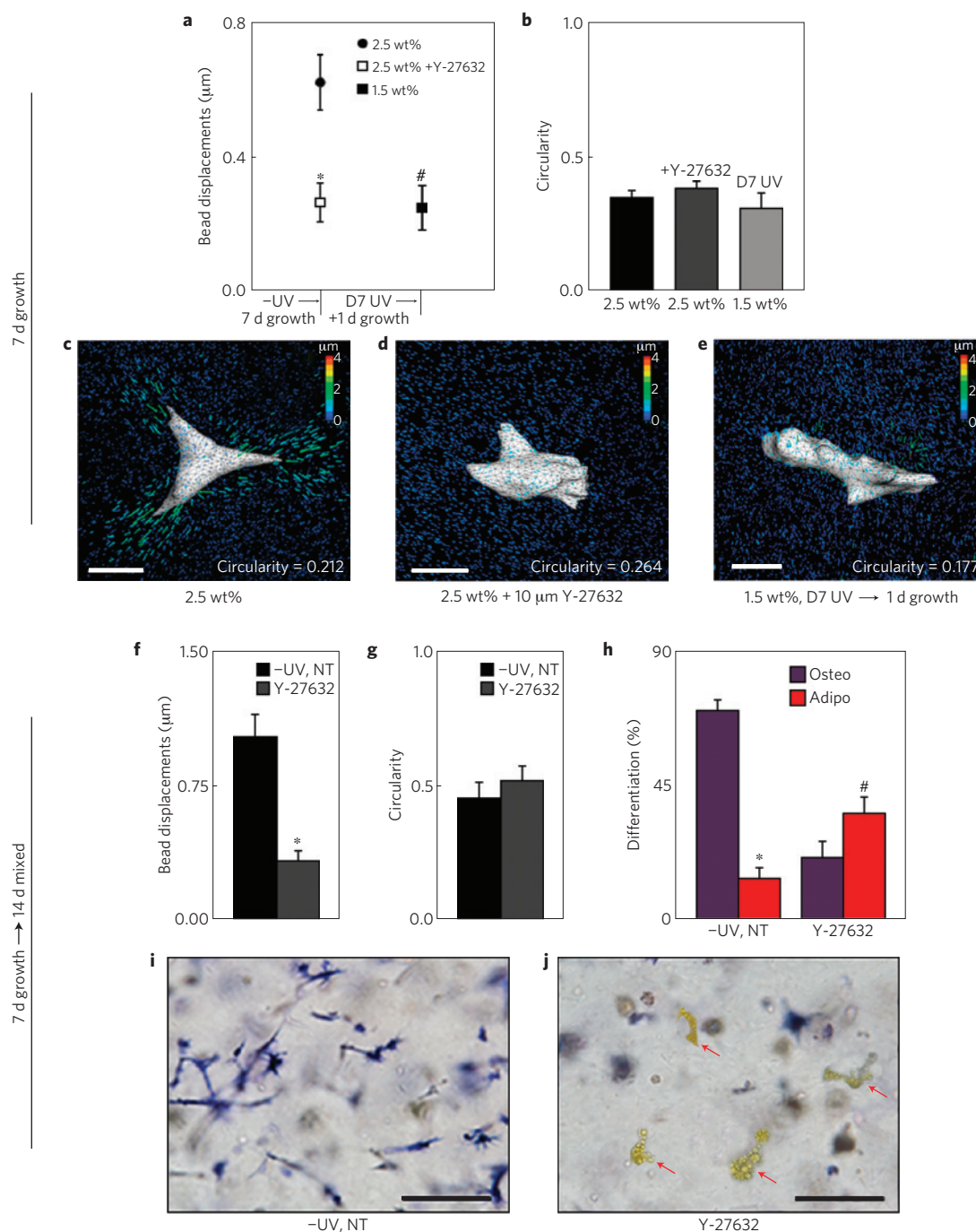


**Figure 5 | hMSC matrix interactions and lineage commitment following pharmacologically induced changes in cytoskeletal tension.** **a,b**, Cell-induced bead displacements ( $*p < 0.001$ ,  $\#p < 0.005$  relative to 2.5 wt%, *t*-test; **a**) and circularity analysis (**b**) of hMSCs within 2.5 wt% -UV MeMaHA gels following 7 d growth-media incubation with or without (no treatment, NT) daily 10  $\mu$ M Y-27632, or within 1.5 wt% D7 UV MeMaHA gels plus one further day growth-media incubation. **c,d**, Representative TFM images of hMSCs within 2.5 wt%, -UV MeMaHA hydrogels following 7 d growth-media incubation either without (**c**) or with (**d**) daily 10  $\mu$ M Y-27632. **e**, Representative TFM image of a hMSC within a 1.5 wt%, D7 UV hydrogel. **f-h**, Cell-induced bead displacements ( $*p < 0.001$  relative to 2.5 wt%, *t*-test; **f**), circularity analysis (**g**) and percentage differentiation fate (**h**) of hMSCs towards osteogenic or adipogenic lineages within 2.5 wt% -UV MeMaHA gels following a further 14 d mixed-media incubation. **i,j**, Representative bright-field images of these same groups stained for ALP (osteogenesis); lipid-containing cells (red arrows) appear yellow. Error bars represent standard error of the mean. Scale bars, 25  $\mu$ m (**c-e**) and 50  $\mu$ m (**i,j**).

morphology (Fig. 5g) were again observed when compared with hMSCs. However, a fate switch from primarily osteogenesis to adipogenesis was also observed through biochemical staining for ALP (Fig. 5i,j) and quantification (Fig. 5h), similar to that observed when non-degradable crosslinks were introduced with D7 UV exposure. Also similar to D7 UV gels, lipid-filled hMSCs within

the -UV Y-27632-treated gels exhibited minimal cytoskeletal organization relative to hMSCs within untreated gels (Supplementary Fig. S18). To rule out off-target effects of the pharmacologic inhibitor, hMSCs in 2.5 wt% -UV gels also were treated with an inhibitor of non-muscle myosin II, blebbistatin, during the differentiation phase (Supplementary Fig. S19). Blebbistatin

(50  $\mu\text{M}$ ) treatment also significantly reduced cellular tractions and osteogenesis, and increased adipogenesis, although to a less pronounced extent relative to the Y-27632 treatment. In addition to its effects on myosin, Y-27632 inhibition of ROCK has been shown also to destabilize F-actin through inhibition of LIM kinase and cofilin, further amplifying its effects<sup>32,33</sup>. Furthermore, a recent report implicated ROCK-induced cytoskeletal tension as a necessary component in hMSC osteogenesis<sup>14,34</sup>. In contrast, blebbistatin acts specifically to inhibit non-muscle myosin-II (refs 35, 36); although this is a primary myosin isoform upregulated in hMSC osteogenesis, recent reports have implicated that multiple myosin isoforms, including smooth muscle myosin<sup>37</sup>, may also be active during osteogenesis. Taken together, these findings suggest that the introduction of non-degradable crosslinks mediates a switch in hMSC behaviour and fate by blocking traction generation in a manner similar to direct pharmacological inhibition of myosin activity.

Collectively, the present work provides new insights into the role of traction generation in hMSC fate choice in 3D hydrogels. Within covalently crosslinked hydrogels in particular, traction is dependent on hMSCs being able to degrade their surroundings and assemble focal adhesions and cytoskeletal structures. Unlike cell behaviour atop 2D substrates, these results highlight the importance of degradability as a parameter separate from the previously described effects of substrate crosslinking or cell morphology. Furthermore, the work stresses the importance of understanding stem cell interactions with each hydrogel type (for example, covalently versus ionically crosslinked), whose degradability and molecular structure may drive divergent outcomes and ultimately impact the successful design of hydrogels in stem-cell-based therapies.

## Methods

For quantification of hMSC differentiation fate and circularity,  $n \geq 45$  cells per condition were analysed. All other experiments were performed in quadruplicate ( $n = 4$ ). For further methods, see Supplementary Information.

**Encapsulation of hMSCs within HA hydrogels.** Previously described methods were used to synthesize MeHA (ref. 30;  $\sim 92\%$  methacrylation) from sodium hyaluronate (Lifecore), MeAlg ( $\sim 70\%$  modification) from sodium alginate (Sigma), and MeDex ( $\sim 50\%$  modification) from dextran (Sigma). MeMaHA with  $\sim 14\%$  and  $\sim 10.5\%$  methacrylate and maleimide modification, respectively, was synthesized through the coupling of the tetrabutylammonium salt of NaHA (HA-TBA) with 2-aminoethyl methacrylate hydrochloride (Sigma) and *N*-(2-aminoethyl)maleimide trifluoroacetate salt (Sigma; Supplementary Fig. S20). The chemical structures and <sup>1</sup>H NMR spectra of MeHA, MeAlg, MeDex and MeMaHA are provided in Supplementary Figs S21–S24, respectively. The integrin-binding peptide GCGYRGD SPG (Genscript; italics indicates the cell-adhesive domain) was conjugated to MeHA, MeAlg and MeDex (754  $\mu\text{M}$ , matching that used in the described physically crosslinked alginate studies), and to MeMaHA (1 mM) through 30 min reaction in pH 8.0 PBS at 25 °C before crosslinking. Passage 3 hMSCs (Lonza) were encapsulated either into MeMaHA (1 million hMSCs ml<sup>-1</sup>) hydrogels using Michael addition reactions between MeMaHA maleimides and the MMP degradable peptide GCRDVP MS↓MRGGDRCG (Genscript; down arrow indicates cleavage site by MMP-2), or into MeHA, MeAlg or MeDex (15 million hMSCs ml<sup>-1</sup>) using photoinitiated free-radical polymerization (Exfo Omnicure S1000 lamp with a 320–390 nm filter, exposure of 10 mW cm<sup>-2</sup> for 5 min) in the presence of 0.05 wt% Irgacure 2959 (I2959; Ciba), a photoinitiator chosen for its aqueous solubility and good cytocompatibility<sup>38</sup>. For CD44 blocking studies, hMSCs were incubated with anti-CD44 (3:1,000, mouse monoclonal antibody CD44, Abcam) in a buffer (2 mM EDTA and 2% FBS in PBS) for 45 min on ice, washed twice in buffer, and resuspended in growth media before encapsulation. All gels were transferred to FBS-supplemented MEM- $\alpha$  (Invitrogen). MeMaHA hydrogels were secondarily photopolymerized at day 0 (D0 UV) or day 7 (D7 UV) by incubating with I2959 and exposing to UV light as described above. The elastic modulus of the hydrogels was measured by parallel-plate compression testing at 10% ramped strain min<sup>-1</sup> as previously reported<sup>27</sup>. For differentiation studies, following 7 days of incubation in growth media, hydrogels were transferred to a 1:1 mixture of adipogenic/osteogenic media (R&D Systems), with media changes every 3 days. For ROCK inhibition studies, selected –UV gels were treated with 10  $\mu\text{M}$  Y-27632 (Sigma) daily during either the growth media (day 1–7) or mixed media (day 7–21) incubation periods.

**Assessment of hMSC matrix interactions, differentiation, viability and proliferation.** To evaluate the extent of matrix adhesions, hMSCs transfected with lentiviral vinculin conjugated with GFP were encapsulated into MeHA and MeMaHA hydrogels. After growth- and/or mixed-media incubation, the gels were fixed in 4% formalin and stained for actin using rhodamine-phalloidin (Invitrogen). For lineage analysis following 7 d (MeHA gels) or 14 d (MeMaHA gels) mixed-media incubation, encapsulated hMSCs were stained for biochemical markers ALP (Fast Blue) and neutral lipid droplets (Oil Red O) as previously reported<sup>9,27</sup>. The differentiation trends were confirmed by immunocytochemistry for OC and FABP, also as previously reported<sup>27</sup>. Percentage differentiation towards each lineage was quantified by counting the number of positively stained cells and dividing by total nuclei. hMSC viability following 7 d growth-media incubation in either –UV, D0 UV or –UV + light (in the absence of photoinitiator) hydrogels was assessed using a live/dead staining kit (Molecular Probes) and reporting (number of viable cells)/(number of total cells). To evaluate proliferation, total double-stranded DNA content was determined using the PicoGreen assay as previously reported<sup>39</sup>.

**Three-dimensional TFM analysis.** Round cover slides were functionalized with methacrylate groups as previously reported<sup>30</sup>. Immediately before crosslinking, MeHA and MeMaHA solutions with 60,000 hMSCs ml<sup>-1</sup> were pipetted between the slide and a sterilized polydimethylsiloxane mould to immobilize the gel to the slide. Two types of fluorescent beads (0.2- $\mu\text{m}$ -diameter, non-functionalized yellow-green (Polysciences) and Suncoast yellow (Bangs Labs)) were co-encapsulated at  $\sim 2 \times 10^{10}$  beads ml<sup>-1</sup> each. Encapsulated cells were imaged using an inverted microscope (Olympus IX71) equipped with a spinning-disc confocal scan head (Yokogawa Electric) and live-cell incubator (Pathology Devices). A 151  $\times$  151  $\times$  200  $\mu\text{m}$  volume was imaged around each cell before and 45 min following cell lysis with 0.5% SDS (Bio-Rad). 2D rendering of the cell surface using image processing software (Amira) and fluorescent-bead displacement tracking using a feature-vector-based algorithm (Matlab) were then performed as previously reported<sup>40</sup>. Further details can be found in the Supplementary Information.

**Cell circularity analysis.** A dimensionless term describing the roundness of encapsulated hMSCs was developed (Supplementary Fig. S6). The distance of each cell surface node to the centre of a box inscribing the cell was calculated and normalized to the maximum distance over all nodes. Circularity was then calculated as the standard deviation of these normalized values multiplied by a scaling constant. As a result, the circularity range is from 0, representing the maximally non-circular cell across all studies, to 1, corresponding to a perfect sphere. Further quantitative details and examples can be found in Supplementary Fig. S6.

Received 14 May 2012; accepted 31 January 2013; published online 24 March 2013

## References

- Nuttelman, C. R., Tripodi, M. C. & Anseth, K. S. Synthetic hydrogel niches that promote hMSC viability. *Matrix Biol.* **24**, 208–218 (2005).
- Ruoslahti, E. & Reed, J. C. Anchorage dependence, integrins, and apoptosis. *Cell* **77**, 477–478 (1994).
- VandeVondele, S., Vörös, J. & Hubbell, J. A. RGD-grafted poly-L-lysine-graft-(polyethylene glycol) copolymers block non-specific protein adsorption while promoting cell adhesion. *Biotechnol. Bioeng.* **82**, 784–790 (2003).
- Docheva, D., Popov, C., Mutschler, W. & Schieker, M. Human mesenchymal stem cells in contact with their environment: Surface characteristics and the integrin system. *J. Cell Mol. Med.* **11**, 21–38 (2007).
- Meredith, J. E. Jr, Fazeli, B. & Schwartz, M. A. The extracellular matrix as a cell survival factor. *Mol. Biol. Cell* **4**, 953–961 (1993).
- Guilak, F. *et al.* Control of stem cell fate by physical interactions with the extracellular matrix. *Cell Stem Cell* **5**, 17–26 (2009).
- Reilly, G. C. & Engler, A. J. Intrinsic extracellular matrix properties regulate stem cell differentiation. **43**, 55–62 (2010).
- Engler, A. J., Sen, S., Sweeney, H. L. & Discher, D. E. Matrix elasticity directs stem cell lineage specification. *Cell* **126**, 677–689 (2006).
- Guvendiren, M. & Burdick, J. A. Stiffening hydrogels to probe short- and long-term cellular responses to dynamic mechanics. *Nature Commun.* **3**, 792 (2012).
- Fu, J. *et al.* Mechanical regulation of cell function with geometrically modulated elastomeric substrates. *Nature Methods* **7**, 733–736 (2010).
- Gilbert, P. M. *et al.* Substrate elasticity regulates skeletal muscle stem cell self-renewal in culture. *Science* **329**, 1078–1081 (2010).
- Guvendiren, M. & Burdick, J. A. The control of stem cell morphology and differentiation by hydrogel surface wrinkles. *Biomaterials* **31**, 6511–6518 (2010).
- Kilian, K. A., Bugarija, B., Lahn, B. T. & Mrksich, M. Geometric cues for directing the differentiation of mesenchymal stem cells. *Proc. Natl Acad. Sci. USA* **107**, 4872–4877 (2010).

14. McBeath, R., Pirone, D. M., Nelson, C. M., Bhadriraju, K. & Chen, C. S. Cell shape, cytoskeletal tension, and RhoA regulate stem cell lineage commitment. *Dev. Cell* **6**, 483–495 (2004).
15. Ruiz, S. A. & Chen, C. S. Emergence of patterned stem cell differentiation within multicellular structures. *Stem Cells* **26**, 2921–2927 (2008).
16. Huebsch, N. *et al.* Harnessing traction-mediated manipulation of the cell/matrix interface to control stem-cell fate. *Nature Mater.* **9**, 518–526 (2010).
17. Benoit, D. S., Schwartz, M. P., Durney, A. R. & Anseth, K. S. Small functional groups for controlled differentiation of hydrogel-encapsulated human mesenchymal stem cells. *Nature Mater.* **7**, 816–823 (2008).
18. Ferreira, L. S. *et al.* Bioactive hydrogel scaffolds for controllable vascular differentiation of human embryonic stem cells. *Biomaterials* **28**, 2706–2717 (2007).
19. Ifkovits, J. L. & Burdick, J. A. Photopolymerizable and degradable biomaterials for tissue engineering applications. *Tissue Eng.* **13**, 2369–2385 (2007).
20. Mann, B. K., Gobin, A. S., Tsai, A. T., Schmedden, R. H. & West, J. L. Smooth muscle cell growth in photopolymerized hydrogels with cell adhesive and proteolytically degradable domains: Synthetic ECM analogs for tissue engineering. *Biomaterials* **22**, 3045–3051 (2001).
21. Nicodemus, G. D. & Bryant, S. J. Cell encapsulation in biodegradable hydrogels for tissue engineering applications. *Tissue Eng.* **14**, 149–165 (2008).
22. Khetan, S., Katz, J. S. & Burdick, J. A. Sequential crosslinking to control cellular spreading in 3-dimensional hydrogels. *Soft Matter* **5**, 1601–1606 (2009).
23. Burdick, J. A., Chung, C., Jia, X., Randolph, M. A. & Langer, R. Controlled degradation and mechanical behavior of photopolymerized hyaluronic acid networks. *Biomacromolecules* **6**, 386–391 (2005).
24. Erickson, I. E. *et al.* Macromer density influences mesenchymal stem cell chondrogenesis and maturation in photocrosslinked hyaluronic acid hydrogels. *Osteoarthritis Cartilage* **17**, 1639–1648 (2009).
25. Legant, W. R. *et al.* Measurement of mechanical tractions exerted by cells in three-dimensional matrices. *Nature Methods* **7**, 969–971 (2010).
26. Hahn, M. S., Miller, J. S. & West, J. L. Three-dimensional biochemical and biomechanical patterning of hydrogels for guiding cell behavior. *Adv. Mater.* **18**, 2679–2684 (2006).
27. Khetan, S. & Burdick, J. A. Patterning network structure to spatially control cellular remodeling and stem cell fate within 3-dimensional hydrogels. *Biomaterials* **31**, 8228–8234 (2010).
28. West, J. L. & Hubbell, J. A. Polymeric biomaterials with degradation sites for proteases involved in cell migration. *Macromolecules* **32**, 241–244 (1999).
29. Miller, J. S. *et al.* Bioactive hydrogels made from step-growth derived PEG-peptide macromers. *Biomaterials* **31**, 3736–3743 (2010).
30. Marklein, R. A. & Burdick, J. A. Spatially controlled hydrogel mechanics to modulate stem cell interactions. *Soft Matter* **6**, 136–143 (2010).
31. Hudson, J. E. *et al.* A synthetic elastomer based on acrylated polypropylene glycol triol with tunable modulus for tissue engineering applications. *Biomaterials* **31**, 7937–7947 (2010).
32. Maekawa, M. *et al.* Signaling from Rho to the actin cytoskeleton through protein kinases ROCK and LIM-kinase. *Science* **285**, 895–898 (1999).
33. Vardouli, L., Moustakas, A. & Stournaras, C. LIM-kinase 2 and cofilin phosphorylation mediate actin cytoskeleton reorganization induced by transforming growth factor- $\beta$ . *J. Biol. Chem.* **280**, 11448–11457 (2005).
34. Shih, Y. R., Tseng, K. F., Lai, H. Y., Lin, C. H. & Lee, O. K. Matrix stiffness regulation of integrin-mediated mechanotransduction during osteogenic differentiation of human mesenchymal stem cells. *J. Bone Miner. Res.* **26**, 730–738 (2011).
35. Duxbury, M. S., Ashley, S. W. & Whang, E. E. Inhibition of pancreatic adenocarcinoma cellular invasiveness by blebbistatin: A novel myosin II inhibitor. *Biochem. Biophys. Res. Commun.* **313**, 992–997 (2004).
36. Even-Ram, S. *et al.* Myosin IIA regulates cell motility and actomyosin-microtubule crosstalk. *Nature Cell Biol.* **9**, 299–309 (2007).
37. Bennett, K. P. *et al.* Proteomics reveals multiple routes to the osteogenic phenotype in mesenchymal stem cells. *BMC Genom.* **8**, 380 (2007).
38. Williams, C. G., Malik, A. N., Kim, T. K., Manson, P. N. & Elisseeff, J. H. Variable cytocompatibility of six cell lines with photoinitiators used for polymerizing hydrogels and cell encapsulation. *Biomaterials* **26**, 1211–1218 (2005).
39. Singer, V. L., Jones, L. J., Yue, S. T. & Haugland, R. P. Characterization of PicoGreen reagent and development of a fluorescence-based solution assay for double-stranded DNA quantitation. *Anal. Biochem.* **249**, 228–238 (1997).
40. Gao, Y. & Kilfoil, M. L. Accurate detection and complete tracking of large populations of features in three dimensions. *Opt. Express* **17**, 4685–4704 (2009).

### Acknowledgements

This work was supported by funding from a Fellowship in Science and Engineering from the David and Lucile Packard Foundation (J.A.B.), a CAREER award (J.A.B.) and Graduate Research Fellowship (S.K.) from the National Science Foundation, and grant GM74048 from the National Institutes of Health (C.S.C.). The authors would like to thank R. Marklein and C. Choi for helpful discussions and experimental assistance.

### Author contributions

S.K. and J.A.B. conceived the ideas and designed the experiments. S.K., M.G., W.R.L. and D.M.C. conducted the experiments and analysed the data. S.K., W.R.L., C.S.C. and J.A.B. interpreted the data and wrote the manuscript.

### Additional information

Supplementary information is available in the [online version of the paper](#). Reprints and permissions information is available online at [www.nature.com/reprints](http://www.nature.com/reprints). Correspondence and requests for materials should be addressed to J.A.B.

### Competing financial interests

The authors declare no competing financial interests.